COMMUNICATION

High-Spin and Reactive Fe_{13} Cluster with Exposed Metal Sites

Anna G. Scott[a], Diogo Alves Galico[b], Isabel Bogacz[c], Junko Yano*, [c], Muralee Murugesu*, [b], and Theodor Agapie*, [a] (Elizaveta A. Suturina[x], Paul H. Oyala[a])

[a] Anna G. Scott, Paul H. Oyala, Theodor Agapie
Division of Chemistry and Chemical Engineering
California Institute of Technology
Pasadena, California 91125, United States Department
E-mail: tagapie@caltech.edu
[b] Diogo Alves Galico, Muralee Murugesu
Department of Chemistry and Biomolecular Sciences
University of Ottawa
Ottawa, Ontario K1N6N5, Canada
E-mail: m.murugesu@uottawa.ca
[c] Isabel Bogacz, Junko Yano
Molecular Biophysics and Integrated Bioimaging Division
Lawrence Berkeley National Laboratory
Berkeley, California, 94720, United States
E-mail: jyano@lbl.gov
[x] Elizaveta A. Suturina
Department of Chemistry
University of Bath
Claverton Down, Bath BA2 7AY, England
E-mail: e.suturina@bath.ac.uk

Supporting information for this article is given via a link at the end of the document.

Abstract: Atomically defined large metal clusters have applications in new reaction development and preparation of materials with tailored properties. Expanding the synthetic toolbox for reactive high nuclearity metal complexes, we report a new class of Fe clusters, **$Tp^*_4W_4Fe_{13}S_{12}$**, displaying a Fe_{13} core with M-M bonds that has precedent only in main group and late metal chemistry. M_{13} clusters with closed shell electron configurations can show significant stability and have been classified as superatoms. In contrast, **$Tp^*_4W_4Fe_{13}S_{12}$** displays a large spin ground state of $S = 13$. This compound performs small molecule activations involving the transfer of up to 12 electrons resulting in significant cluster rearrangements.

Isolable transition metal-only high nuclearity clusters of well-defined atomic composition and structure are of interest for understanding nanoparticle growth processes and electronic structures, new optical and magnetic properties, designing new materials with tailored properties, tuning reactivity, and modeling heterogeneous catalysts.[1–8] Towards such applications, larger transition metal-only clusters displaying M-M interactions, without supporting interstitial bridging anionic ligands have been prepared for late transition metals, most commonly noble metals, although examples are known for first row transition metals such as Cu and Ni.[5,9–21] Isolation of some of these clusters is proposed to be facilitated by a closed shell electronic configuration that imparts particular stability within the superatom model.[22,23] However, while the structure of numerous large clusters has been determined using single-crystal X-ray diffraction (SC-XRD), use of such clusters to gain atomic level insight into reactivity on the surface of clusters has typically been hindered by the saturated coordination sphere and the propensity of complex clusters to fragment into smaller species.[23,24]

Toward developing new reactivity, synthetic protocols for larger clusters with open coordination sites for reaction chemistry and a greater number of metal-metal interactions are desirable.[25,26] Synthetic procedures for clusters of transition metals typically use metal salt precursors in combination with reducing agents and organic ligands.[1,7,9,27–29] Modification of known clusters has been demonstrated as a complementary route to new complexes.[10,12,30] Assembly of tetranuclear iron sulfur clusters into oligomers upon halide abstraction or reduction provides precedent for employing small clusters to generate higher complexity structures, though typically containing interstitial bridges.[31,32] Herein, we employ a tetranuclear precursor **$[Et_4N]_2[Tp^*WFe_3S_3(u_3\text{-}Cl)Cl_3]$**[33] as a building unit to a more complex cluster, **$Tp^*_4W_4Fe_{13}S_{12}$**, with an unprecedented Fe_{13} core. **$Tp^*_4W_4Fe_{13}S_{12}$**, a cluster with large spin ground state, displays open coordination sites and is reactive, yet sufficiently stabilized to allow the isolation of small molecule activation products including complexes with surface nitride, imide, and sulfide groups.

Toward lower oxidation state high nuclearity clusters for reductive reactivity, we employed precursors anchored by the robust Tp^*WS_3 unit (Tp^* = tris(3,5-dimethyl-1-pyrazolyl)borate).[34] Taking advantage of the lability of the chloride ligands in the presence of a halide abstracting reagent in comparison to the thiolate, phosphine, carbene, sulfide, or nitride ligands of previously reported clusters,[31,33] we previously developed reduction chemistry starting from **$[Et_4N]_2[Tp^*WFe_3S_3(\mu_3\text{-}Cl)Cl_3]$**[33] (Figure 1A, Et_4N = tetraethylammonium) to access $Tp^*WFe_3S_3$ complexes supported by carbene ligands (L) with Fe_3 open faces.[35] To generate higher nuclearity clusters, reduction was performed in the absence of additional supporting ligands L that could trap small metal clusters.

Treatment of **$[Et_4N]_2[Tp^*WFe_3S_3(\mu_3\text{-}Cl)Cl_3]$** with reductant and halogen abstracting reagent results in a cluster with the overall chemical formula **$Tp^*_4W_4Fe_{13}S_{12}$** as determined by SC-XRD (Figure 1A). **$Tp^*_4W_4Fe_{13}S_{12}$** consists of four Tp^*WS_3 units tetrahedrally arranged (Figure 1D) around a pseudo-icosahedral

Fe_{12} core with an additional Fe atom bound in the center.[36] The Fe-Fe distances are between 2.395(2) and 2.771(2) Å (Table S1), within the range of metal-metal bonds for molecular Fe complexes.[37,38] The W-S distances match the parameters observed for reduced Tp*WFe_3S_3 clusters supported by NHC ligands at Fe.[35] The Fe-S bonds show a significant lengthening relative to the precursor, consistent with reduction at Fe.[39] Overall, the 17 metal centers

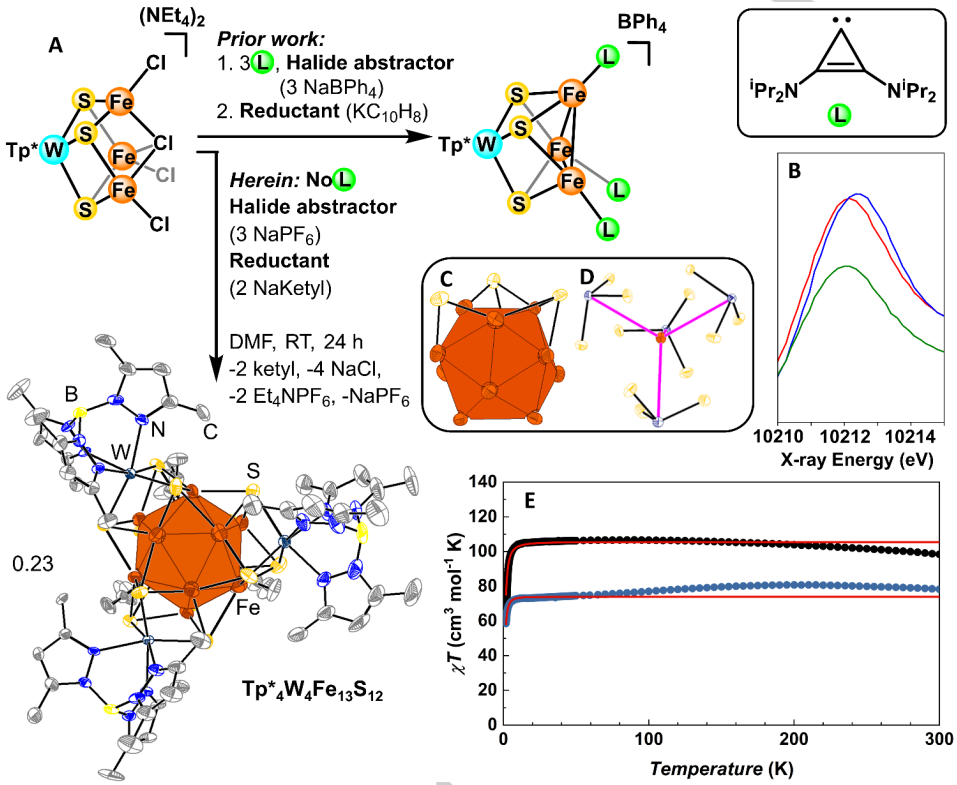

Figure 1. (A) Synthesis of **Tp*$_4$W$_4$Fe$_{13}$S$_{12}$**. Solvent and hydrogen atoms omitted for clarity and ellipsoids plotted at the 50% probability level. (B) W L_3 XANES data for **[Et$_4$N]$_2$[Tp*WFe$_3$S$_3$(μ_3-Cl)Cl$_3$]** (green), **Tp*$_4$W$_4$Fe$_{13}$S$_{12}$** (red), and **Tp*$_4$W$_4$Fe$_{13}$S$_{12}$N$_4$** (blue). (C) Fe_{13} core highlighting one Fe_3S_3 cavity motif. (D) Tetrahedral arrangement of 4 WS_3 units around the central Fe atom of the Fe_{13} core. (E) Direct current variable temperature magnetic susceptibility measurements for **Tp*$_4$W$_4$Fe$_{13}$S$_{12}$** (black circles) ~~) and **Tp*$_4$W$_4$Fe$_{13}$S$_{14}$** (blue circles)~~ collected from 1.8 to 300 K, after diamagnetic correction. Red lines corresponds to the best fitting using PHI software (*S* = 13, *D* = -0.6 cm^{-1}, and *g* = 2.15).[40] ~~For **Tp*$_4$W$_4$Fe$_{13}$S$_{12}$**, *S* = 13, *D* = -0.6 cm^{-1}, and *g* = 2.15. For **Tp*$_4$W$_4$Fe$_{13}$S$_{14}$**, *S* = 13, *D* = -0.16 cm^{-1}, and *g* = 1.80~~.

Formatted: Font: Italic

Commented [A1]: Need to change figure to remove blue data

carry a 28+ charge, M_{17}^{28+}. There are four open Fe_3 faces, each with three surrounding bridging sulfides that create a cavity around these potential binding sites (Figure 1C, S2).

The icosahedral metal cluster motif is known for transition metals past group 8.[10,41,42] Lower symmetry reduced clusters of group 8 metals, Ru_{10} and Os_{20},[43,44] have been reported, but are coordinately saturated with CO ligands. Icosahedral M_{13} clusters of main group and later transition metals, including $[Al_{13}]^-$, $[Au_{13}]^{5+}$, $[Cu_{13}]^{5+}$, have been reported to be particularly robust and are described as metallic superatoms due to their closed shell electronic structure in the Jellium model and full shell of 12 atoms around the central metal.[1,10,45] To probe the open shell nature of **Tp*$_4$W$_4$Fe$_{13}$S$_{12}$** direct current (dc) susceptibility measurements were performed on a polycrystalline sample restrained in grease to prevent torquing (see SI). At room temperature, a χT value of 98.39 cm^3 K mol^{-1} is observed (Figure 1E), which suggests the presence of S = 13 ground state open shell system. It is reasonable to assume all the spins within the clusters are strongly coupled even at room temperature, given the metal-metal bonded core within the cluster. Upon reducing the temperature, the χT product slightly increases to 106.67 cm^3 K mol^{-1} at 80 K. Such behavior was also previously seen for the hexanuclear metal-metal bonded Fe clusters.[46–48] The χT product remains relatively constant down to 10 K; thereafter it decreases rapidly to reach a

minimum value of 58.89 cm^3 K mol^{-1} at 1.8 K. The low temperature behavior is likely due to zero-field splitting. To probe further, magnetization measurements at variable fields (0-7 T) in the temperature range of 2-9 K were performed on **$Tp^*_4W_4Fe_{13}S_{12}$**. Fitting of the data using PHI software[40] afforded a ground spin state of S = 13 (g = 2.15 and D = -0.6 cm^{-1}, Figure 1E and S4). An electron paramagnetic resonance study of **$Tp^*_4W_4Fe_{13}S_{12}$** reveals transitions in both parallel and perpendicular modes and fitting of the data yields S = 13 (g = 1.9, D = - 0.2 cm-1, and E/D = 0.013; Figure S6 and S7). These results clearly set this system apart from the previously reported closed shell metallic superatoms.

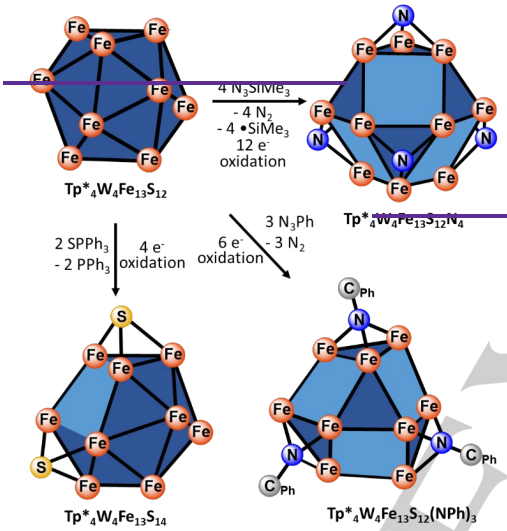

To address electron distribution within the cluster, X-ray absorption near edge spectroscopy (XANES) experiments were performed on **$[Et_4N]_2[Tp^*WFe_3S_3(\mu_3\text{-}Cl)Cl_3]$** and **$Tp^*_4W_4Fe_{13}S_{12}$** to probe the W L_2 and L_3 edge, considering that the coordination sphere of W is maintained across these clusters (Figure 1B, S5). Peak centers remain at 10214.2 eV for both clusters, while there is a less than 0.1 eV white line shift for L_2 and no shift for L_3. Assuming an oxidation state for **$[Et_4N]_2[Tp^*WFe_3S_3(\mu_3\text{-}Cl)Cl_3]$** as W(III),[49,50] a similar effective charge is maintained for **$Tp^*_4W_4Fe_{13}S_{12}$** according to the XANES data, although further studies are needed to conclusively assign the oxidation state.[51,52] Given this tentative W(III) assignment, the formal charge distribution on Fe is $[Fe_{13}]^{16+}$, placing 88 electrons in Fe d-based molecular orbitals. With only three weak field ligands coordinated to each outer Fe center, low d-d splitting is expected. Within the d-based molecular orbital manifold for the Fe-Fe and Fe-S interactions, the highest spin state corresponds to 42 unpaired electrons for $[Fe_{13}]^{16+}$. A sufficiently large orbital splitting resulting in an intermediate spin orbital population in combination with antiferromagnetic interactions with the four W centers[53,54] could bring the spin value of **$Tp^*_4W_4Fe_{13}S_{12}$** in the range estimated from the magnetization data.

*Quantum chemistry calculations of different spin states (from S=1 to S=37) at BP86/def2-SVP level of theory done ~~on~~using the XRD structure of **$Tp^*_4W_4Fe_{13}S_{12}$** suggest that the lowest energy state has a considerably high total spin of S=16 (Figure 2, Table S3); the experimentally determined S = 13 is close in energy. In S=16 state, the Mulliken spin population on W is -0.8/-0.9 suggesting that each tungsten carries one unpaired electron with the spin antiparallel to the spin of Fe_{13} core. This is consistent with low-spin W(III). All spins of Fe centres are aligned with each other, and spin population is 2.7/2.8 on prereferral ions while the Fe center in the middle of the cluster has the spin population of 1.5. Magnetic moment per Fe atom is close to the calculated values for neutral and mono cationic/anionic Fe clusters of various sizes despite much smaller number of electrons in the formally $[Fe_{13}]^{16+}$ core.[55]*

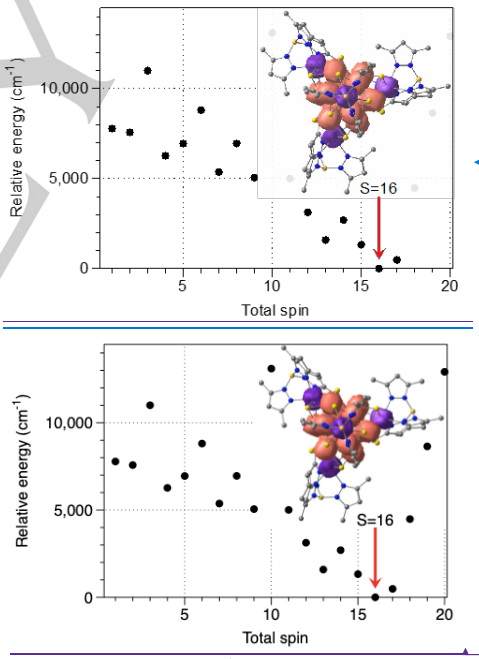

Figure 2. Relative energies (in cm^{-1}) of spin states from S=1 to S=20 of **$Tp^*_4W_4Fe_{13}S_{12}$** complex calculated with BP86/def2-SVP level of theory. Inset: XRD structure of the molecule shown along C_3 symmetry axis with the S=16 state (lowest energy) spin density iso-surface (contour value 0.008) where positive value shown in coral colour and negative value shown in purple colour.

Commented [TA5]: Liza, are you ok with this addition?

Commented [ES6R5]: Yes. I'll send my additional thoughts to Diogo and Muralee. You are right that there are a few spin states which are quite close, and the DFT has its limits, so it is possible that a spin state between S=11 to S=18 is actually the lowest one (they are all within 5000 cm-1).

Commented [A7]: Doesn't agree with SQUID/EPR

Commented [ES8R7]: Indeed it could be the calculations that are wrong about the spin state. However we should also keep in mind that it might be possible to fit the SQUID data with higher spin and lower g value (lower than 2.16). And a diamagnetic impurity or error in molecular weight might affect the high temperature limit of chiT data.

Commented [TA9]: Liza, Serena DeBeer has published on W and Mo having a non-Hund electron configuration with two spins up one down, but still all in different orbitals. Is this what your data show?

Commented [ES10R9]: It could the case. However I need CASSCF calculation to talk about the electron configuration in a rigorous way, sadly my few attempts to converge CASSCF for a single W site were not successful.

Formatted: Highlight

Formatted: Highlight

Formatted: Highlight

Commented [A11]: Would this be consistent with the XANES data? It is still W(III), but now low spin.

Commented [A2]: Will need to discuss with Diogo and Muralee to see what they think about this comparison.

Commented [A12]: Doesn't agree with SQUID/EPR

Commented [A13]: Would this be consistent with the XANES data? It is still W(III), but now low spin.

Formatted: German (Germany)

Formatted: Centered

Formatted: German (Germany)

Formatted: Font: 7 pt, Bold, Italic

Formatted: Font: 7 pt

Commented [TA3]: Liza, are the structural parameters reproduced reasonably well? It would be good to mention that.

Commented [ES4R3]: I have used the XRD data (no geometry optimisation) as gas phase optimised structure could lead to different magnetic properties and won't be comparable with solid-state experiments (SQUID/ powder EPR)

Formatted: Font: 7 pt, German (Germany)

Formatted: German (Germany)

~~However, with the complexity given by the presence of three types of metal centers, two for Fe (the central atom and the twelve peripheral atoms) and one for W, additional studies will be necessary to interpret the electronic structure and magnetism of this compound.~~ Clusters with notably high spin values are typically generated from higher nuclearity clusters with bridging ligands, such as oxides, that facilitate superexchange pathways for spin coupling.[56–59] However, these weak interactions are overcome at high temperatures. Stronger coupling can be achieved through a molecular orbital manifold in complexes with intermediate strength metal-metal interactions resulting in moderate splitting of the d-based orbitals, where the cluster is conceptually analogous

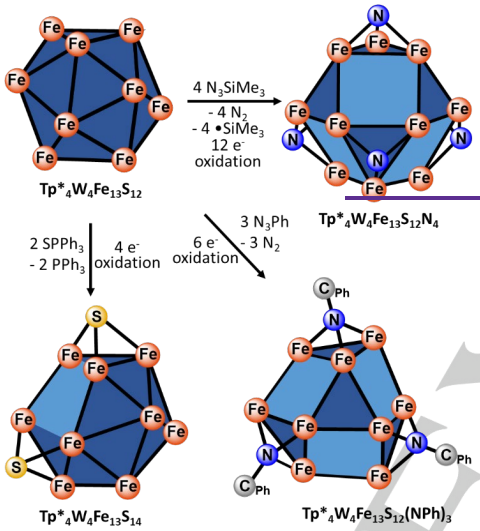

Figure 3: Reactions of $Tp^*_4W_4Fe_{13}S_{12}$. Tp^*WS_3 fragments are not shown for clarity. Triangular and square faces are shown in dark and light blue, respectively.

to a high spin single metal complex.[46,48,60,61] Overall, **$Tp^*_4W_4Fe_{13}S_{12}$** demonstrates a strategy to achieve high spin states through high nuclearity metallic cores terminated with weak field bridging sulfide ligands.

Several aspects of **$Tp^*_4W_4Fe_{13}S_{12}$** suggest potential for reactivity, including a relatively reduced redox state, open coordination sites, a high spin, and metal-metal bonds. The open, coordinately unsaturated Fe_3 faces are reminiscent of triangular motifs known to undergo small molecule activations for M_3 clusters,[37,62,63] including nitrogen atom and nitrene transfer chemistry in up to four electron redox processes.[37,64–67] Such studies have shown that metal-metal interactions can allow for multi-electron redox chemistry without metal centers in particularly low oxidation states. **$Tp^*_4W_4Fe_{13}S_{12}$** has four of these surface Fe_3 structural motifs as well as the additional redox active central Fe atom and distal W centers. Considering that heterogeneous iron catalysts are employed in the Haber Bosch process and insight into the bonding of proposed intermediates of N_2 reduction to multimetallic sites is limited,[68,69] we targeted reactions with nitrogeneous ligands. Reaction of **$Tp^*_4W_4Fe_{13}S_{12}$** with four equivalents of trimethylsilylazide (N_3SiMe_3) results in the transfer of four nitride atoms (Figure 32) to generate **$Tp^*_4W_4Fe_{13}S_{12}N_4$** in an overall 12 electron process, a remarkable number for a single molecule. The Fe_{13} core has been converted from a centered icosahedron to a centered cuboctahedron (Figure 23, 34).[10,45] Despite the substantial reorganization of the Fe_{13} core and the formal transfer of 12 electrons, the Fe-Fe distances (2.568(2)-2.737(2) Å, Table S1) remain within the range of the starting material suggesting a propensity to maintain metal-metal interactions. The W-S bond lengths shorten slightly, to an average length of 2.331(9) Å,

~~***Figure 2***: Reactions of $Tp^*_4W_4Fe_{13}S_{12}$. Tp^*WS_3 fragments are not shown for clarity. Triangular and square faces are shown in dark and light blue, respectively.~~

suggesting partial oxidation at W. DFT studies of the relative stability of gas phase metal clusters without supporting ligands[70]

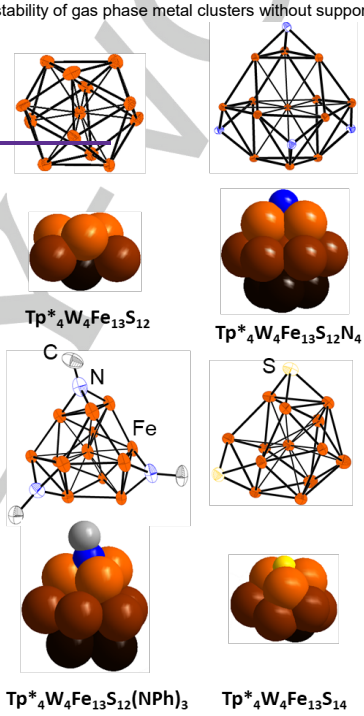

indicate that the metal oxidation states impact the energies of various cluster geometries, of potential consequence here given the redox changes between M_{17}^{28+} and M_{17}^{40+}. Comparison of **$Tp^*_4W_4Fe_{13}S_{12}$** and **$Tp^*_4W_4Fe_{13}S_{12}N_4$** demonstrates that cluster reorganization remains possible in the presence of surface ligands, where the energetics of metal-ligand interactions on geometry must be taken into account. For example, whereas the sulfides of the Tp^*WS_3 fragments each bind trigonal Fe_3 faces in **$Tp^*_4W_4Fe_{13}S_{12}$**, they coordinate to Fe-Fe edges of Fe_4 squares in **$Tp^*_4W_4Fe_{13}S_{12}N_4$** (Figure ~~S6~~S8). Compared to **$Tp^*_4W_4Fe_{13}S_{12}$**, **$Tp^*_4W_4Fe_{13}S_{12}N_4$** exhibits a white line shift of 1.5 eV for the W L_2 edge and 1.0 eV for the W L_3 edge (Figure 1B, S5). While this indicates a change in charge density at W, which is remote from

Field Code Changed

Formatted: Font: Italic

the site of reaction chemistry at Fe, further studies are needed to assign formal oxidation state changes.

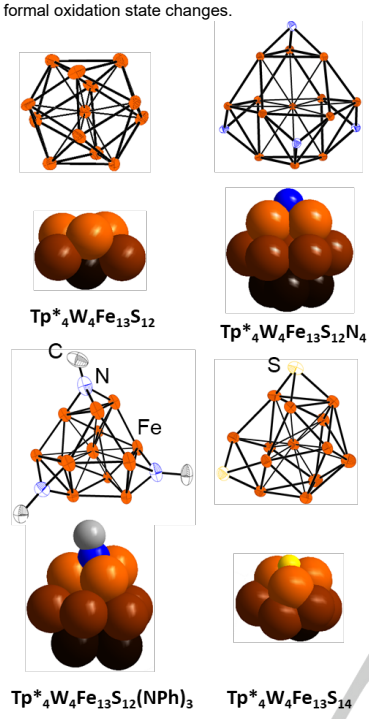

Figure 4: Thermal ellipsoid plots of Fe_{13} cores with substrate molecules bound for $Tp^*_4W_4Fe_{13}S_{12}$, $Tp^*_4W_4Fe_{13}S_{12}N_4$, $Tp^*_4W_4Fe_{13}S_{12}(NPh)_3$, and $Tp^*_4W_4Fe_{13}S_{14}$ and space filling models for one Fe_3 face of each cluster with one of bound substrate molecules and adjacent Fe atoms shown in different shades of orange based on layer. Ellipsoids are plotted at the 50% probability level.

To gain access to an imide analog of **$Tp^*_4W_4Fe_{13}S_{12}N_4$** for comparison, reactions with phenyl azide (PhN_3) were performed. Treatment of **$Tp^*_4W_4Fe_{13}S_{12}$** with three equivalents of PhN_3 resulted in the isolation of the tris-imide species **$Tp^*_4W_4Fe_{13}S_{12}(NPh)_3$**. Again, all of the atoms of the cluster precursor are maintained, and the geometry is altered toward a centered cuboctahedral geometry, but with substantial distortions (Figure 3, 4).

Despite the redox state and Fe_{13} structure being between those of **$Tp^*_4W_4Fe_{13}S_{12}$** and **$Tp^*_4W_4Fe_{13}S_{12}N_4$**, **$Tp^*_4W_4Fe_{13}S_{12}(NPh)_3$** displays Fe-Fe distances that are longer than both (up to 2.941(5) Å compared to 2.737(2) and 2.771(2) Å, respectively). This observation indicates that the M-M distances are not directly predicated by the redox state of the metal. In fact, the cluster of intermediate oxidation state has the longest M-M distance.

~~**Figure 3**: Thermal ellipsoid plots of Fe_{13} cores with substrate molecules bound for $Tp^*_4W_4Fe_{13}S_{12}$, $Tp^*_4W_4Fe_{13}S_{12}N_4$, $Tp^*_4W_4Fe_{13}S_{12}(NPh)_3$, and $Tp^*_4W_4Fe_{13}S_{14}$ and space filling models for one Fe_3 face of each cluster with one of bound substrate molecules and adjacent Fe atoms shown in different shades of orange based on layer. Ellipsoids are plotted at the 50% probability level.~~

To further explore the impact of the group transferred on the cluster structure, installation of sulfide was targeted, as a ligand isolobal to both nitride and imide. **$Tp^*_4W_4Fe_{13}S_{12}$** reacts with two equivalents of triphenylphosphine sulfide ($SPPh_3$) to form **$Tp^*_4W_4Fe_{13}S_{14}$** (Figure 3), as observed by SC-XRD and the byproduct PPh_3 (^{31}P NMR spectroscopy, Figure S108). Two sulfur atoms have been transferred, in contrast to three and four for the reactions with PhN_3 and Me_3SiN_3, respectively, in a four electron redox process. The Fe_{13} core of the product has lower symmetry and becomes distorted from an icosahedron such that two of the Fe-Fe distances increase to greater than 3 Å (Figure 3 and 4). ~~Magnetic data were also measured for **$Tp^*_4W_4Fe_{13}S_{14}$** with the goal to understanding the impact of the sulfide addition on the overall magnetic properties. At room temperature, a lowering of the χT value to 78.28 $cm^3 K mol^{-1}$ is observed (Figure 1E). However, fitting of the data also suggests the presence of S = 13 ground state open shell system (g = 1.8 and D = -0.16 cm^{-1}, Fig. 1E, and S11). Despite the fact that **$Tp^*_4W_4Fe_{13}S_{14}$** and **$Tp^*_4W_4Fe_{13}S_{12}$** differ by four electrons, their spin states are estimated to be the same. This could be a consequence of changes in electronic structure induced by the two additional sulfide ligands for example by altering the population of the d-orbital manifold of the Fe_{13} core, which highlights a strategy to tune the magnetism of these compounds with the surface ligands.~~

Analysis of the multiiron layers below an open triangular Fe_3 face in the precursor (**$Tp^*_4W_4Fe_{13}S_{12}$**) versus a ligand coordinated Fe_3 face in each of the group transfer cluster products shows substantial Fe atom shifts (Figure 4). Notably, the most pronounced variation of Fe-Fe distances within one cluster were observed in the cases where fewer groups and electrons were transferred.

In summary, we report a synthetic strategy for the synthesis of metallic Fe_{13} clusters upon reduction of a tetranuclear precursor, **$[Et_4N]_2[Tp^*WFe_3S_3(\mu_3\text{-}Cl)Cl_3]$**. The atomically precise characterization of **$Tp^*_4W_4Fe_{13}S_{12}$**, **$Tp^*_4W_4Fe_{13}S_{12}N_4$**, **$Tp^*_4W_4Fe_{13}S_{12}(NPh)_3$**, and **$Tp^*_4W_4Fe_{13}S_{14}$** demonstrates that large clusters can maintain the metallic core while performing well-defined multi-electron multiple group transfer chemistry with overall redox changes of 4 to 12 electrons. **$Tp^*_4W_4Fe_{13}S_{12}$** shows notably high spin values at room temperature for metallic clusters, highlighting the potential of this type of coordination compound for magnetic materials applications. The structural variation observed with the present clusters shows the ability of multimetallic systems to accommodate the bonding requirements of large redox and ligand changes. The propensity for surface rearrangement demonstrated with the transfer of nitrogen, nitrene, and sulfur ligands can serve as a tool for new reactive cluster design. The availability of clusters displaying the $Tp^*WM_3S_3$ motif for other transition metals[71] provides a starting point to a broader range of large metallic clusters related to those reported here.

Acknowledgements

We are grateful to the National Institutes of Health (R01-GM102687B to T.A.) and the National Science Foundation (Graduate Research Fellowships Program to A.G.S.) for funding, the Beckman Institute and the Dow Next Generation Grant for instrumentation support, Michael Takase and Lawrence Henling for assistance with crystallography. Part of this work (XAS data collection) was carried out at the Stanford Synchrotron Radiation

Formatted: Centered

Formatted: Space After: 0 pt

Lightsource, SLAC National Accelerator Laboratory, which is supported by the U.S. Department of Energy, Office of Science, Office of Basic Energy Sciences under Contract No. DE-AC02-76SF00515. XAS studies were performed with support of the NIH GM110501 (J.Y.). EAS gratefully acknowledges the University of Bath's Research Computing Group (doi.org/10.15125/b6cd-s854) for their support in this work.

References

[1] E. A. Doud, A. Voevodin, T. J. Hochuli, A. M. Champsaur, C. Nuckolls, X. Roy, *Nat Rev Mater* **2020**, *5*, 371–387.
[2] S. A. Claridge, A. W. Castleman, S. N. Khanna, C. B. Murray, A. Sen, P. S. Weiss, *ACS Nano* **2009**, *3*, 244–255.
[3] N. Yan, Y. Yuan, P. J. Dyson, *Dalton Trans.* **2013**, *42*, 13294–13304.
[4] G. Reiss, A. Hütten, *Nature Mater* **2005**, *4*, 725–726.
[5] Y. Du, H. Sheng, D. Astruc, M. Zhu, *Chemical reviews* **2019**, *120*, 526–622.
[6] D. D. Robertson, M. L. Personick, *Chem. Mater.* **2019**, *31*, 1121–1141.
[7] R. Jin, G. Li, S. Sharma, Y. Li, X. Du, *Chem. Rev.* **2021**, *121*, 567–648.
[8] L. Liu, A. Corma, *Chemical reviews* **2018**, *118*, 4981–5079.
[9] T.-A. D. Nguyen, Z. R. Jones, B. R. Goldsmith, W. R. Buratto, G. Wu, S. L. Scott, T. W. Hayton, *J. Am. Chem. Soc.* **2015**, *137*, 13319–13324.
[10] K. K. Chakrahari, J.-H. Liao, S. Kahlal, Y.-C. Liu, M.-H. Chiang, J.-Y. Saillard, C. W. Liu, *Angewandte Chemie International Edition* **2016**, *55*, 14704–14708.
[11] R. S. Dhayal, J.-H. Liao, X. Wang, Y.-C. Liu, M.-H. Chiang, S. Kahlal, J.-Y. Saillard, C. W. Liu, *Angewandte Chemie International Edition* **2015**, *54*, 13604–13608.
[12] T.-A. D. Nguyen, Z. R. Jones, D. F. Leto, G. Wu, S. L. Scott, T. W. Hayton, *Chem. Mater.* **2016**, *28*, 8385–8390.
[13] M. Sugiuchi, Y. Shichibu, T. Nakanishi, Y. Hasegawa, K. Konishi, *Chem. Commun.* **2015**, *51*, 13519–13522.
[14] A. J. Touchton, G. Wu, T. W. Hayton, *Inorg. Chem.* **2021**, *60*, 17586–17592.
[15] J. G. Brennan, T. Siegrist, Y. U. Kwon, S. M. Stuczynski, M. L. Steigerwald, *J. Am. Chem. Soc.* **1992**, *114*, 10334–10338.
[16] D. Fenske, H. Krautscheid, M. Müller, *Angewandte Chemie International Edition in English* **1992**, *31*, 321–323.
[17] H. Qian, M. Zhu, Z. Wu, R. Jin, *Acc. Chem. Res.* **2012**, *45*, 1470–1479.
[18] H. Yang, Y. Wang, N. Zheng, *Nanoscale* **2013**, *5*, 2674–2677.
[19] A. Desireddy, B. E. Conn, J. Guo, B. Yoon, R. N. Barnett, B. M. Monahan, K. Kirschbaum, W. P. Griffith, R. L. Whetten, U. Landman, T. P. Bigioni, *Nature* **2013**, *501*, 399–402.
[20] J. D. Erickson, E. G. Mednikov, S. A. Ivanov, L. F. Dahl, *J. Am. Chem. Soc.* **2016**, *138*, 1502–1505.
[21] P. Chini, *Journal of Organometallic Chemistry* **1980**, *200*, 37–61.
[22] A. C. Reber, S. N. Khanna, *Acc. Chem. Res.* **2017**, *50*, 255–263.
[23] M. Walter, J. Akola, O. Lopez-Acevedo, P. D. Jadzinsky, G. Calero, C. J. Ackerson, R. L. Whetten, H. Grönbeck, H. Häkkinen, *PNAS* **2008**, *105*, 9157–9162.
[24] D. B. Eremin, V. P. Ananikov, *Coordination Chemistry Reviews* **2017**, *346*, 2–19.
[25] S. Takano, T. Tsukuda, *J. Am. Chem. Soc.* **2021**, *143*, 1683–1698.
[26] H. Yang, Y. Wang, J. Lei, L. Shi, X. Wu, V. Mäkinen, S. Lin, Z. Tang, J. He, H. Häkkinen, L. Zheng, N. Zheng, *J. Am. Chem. Soc.* **2013**, *135*, 9568–9571.
[27] W.-D. Si, Y.-Z. Li, S.-S. Zhang, S. Wang, L. Feng, Z.-Y. Gao, C.-H. Tung, D. Sun, *ACS Nano* **2021**, *15*, 16019–16029.
[28] C. Sun, N. Mammen, S. Kaappa, P. Yuan, G. Deng, C. Zhao, J. Yan, S. Malola, K. Honkala, H. Häkkinen, B. K. Teo, N. Zheng, *ACS Nano* **2019**, *13*, 5975–5986.
[29] M. Zhu, E. Lanni, N. Garg, M. E. Bier, R. Jin, *J. Am. Chem. Soc.* **2008**, *130*, 1138–1139.
[30] E. Ito, S. Takano, T. Nakamura, T. Tsukuda, *Angewandte Chemie International Edition* **2021**, *60*, 645–649.
[31] S. C. Lee, W. Lo, R. Holm, *Chemical reviews* **2014**, *114*, 3579–3600.
[32] G. Xu, J. Zhou, Z. Wang, R. H. Holm, X.-D. Chen, *Angewandte Chemie International Edition* **2019**, *58*, 16469–16473.
[33] G. Xu, Z. Wang, R. Ling, J. Zhou, X.-D. Chen, R. H. Holm, *Proceedings of the National Academy of Sciences* **2018**, *115*, 5089–5092.
[34] B. Zheng, X.-D. Chen, S.-L. Zheng, R. H. Holm, *J. Am. Chem. Soc.* **2012**, *134*, 6479–6490.
[35] L. N. V. Le, G. A. Bailey, A. G. Scott, T. Agapie, *PNAS* **2021**, *118*, e2109241118.
[36] **N.d.**
[37] T. M. Powers, T. A. Betley, *J. Am. Chem. Soc.* **2013**, *135*, 12289–12296.
[38] N. A. Pushkarevsky, S. N. Konchenko, M. Zabel, M. Bodensteiner, M. Scheer, *Dalton Transactions* **2011**, *40*, 2067–2074.
[39] A. Majumdar, R. Holm, *Inorganic chemistry* **2011**, *50*, 11242–11251.
[40] N. F. Chilton, R. P. Anderson, L. D. Turner, A. Soncini, K. S. Murray, *Journal of Computational Chemistry* **2013**, *34*, 1164–1175.
[41] M. Laupp, J. Strähle, *Angewandte Chemie International Edition in English* **1994**, *33*, 207–209.
[42] R. S. Dhayal, J.-H. Liao, Y.-C. Liu, M.-H. Chiang, S. Kahlal, J.-Y. Saillard, C. W. Liu, *Angewandte Chemie International Edition* **2015**, *54*, 3702–3706.
[43] P. J. Bailey, M. A. Beswick, B. F. G. Johnson, J. Lewis, P. R. Raithby, M. C. R. de Arellano, *Journal of the Chemical Society, Dalton Transactions* **1992**, *0*, 3159–3160.
[44] L. H. Gade, B. F. G. Johnson, J. Lewis, M. McPartlin, H. R. Powell, P. R. Raithby, W.-T. Wong, *J. Chem. Soc., Dalton Trans.* **1994**, 521–532.
[45] E. Roduner, *Physical Chemistry Chemical Physics* **2018**, *20*, 23812–23826.
[46] R. H. Sánchez, T. A. Betley, *J. Am. Chem. Soc.* **2018**, *140*, 16792–16806.
[47] J. Nehrkorn, S. M. Greer, B. J. Malbrecht, K. J. Anderton, A. Aliabadi, J. Krzystek, A. Schnegg, K. Holldack, C. Herrmann, T. A. Betley, S. Stoll, S. Hill, *Inorg. Chem.* **2021**, *60*, 4610–4622.
[48] R. Hernández Sánchez, T. A. Betley, *J. Am. Chem. Soc.* **2015**, *137*, 13949–13956.
[49] D. Hong, Y. Zhang, R. H. Holm, *Inorganica chimica acta* **2005**, *358*, 2303–2311.
[50] C. Hauser, E. Bill, R. H. Holm, *Inorg. Chem.* **2002**, *41*, 1615–1624.
[51] J. K. Kowalska, A. W. Hahn, A. Albers, C. E. Schiewer, R. Bjornsson, F. A. Lima, F. Meyer, S. DeBeer, *Inorg. Chem.* **2016**, *55*, 4485–4497.
[52] U. Jayarathne, P. Chandrasekaran, A. F. Greene, J. T. Mague, S. DeBeer, K. M. Lancaster, S. Sproules, J. P. Donahue, *Inorg. Chem.* **2014**, *53*, 8230–8241.
[53] R. Bjornsson, F. A. Lima, T. Spatzal, T. Weyhermüller, P. Glatzel, E. Bill, O. Einsle, F. Neese, S. DeBeer, *Chemical Science* **2014**, *5*, 3096–3103.

Formatted: Font: 11 pt, Bold

Formatted: Font: (Default) Arial, 8.5 pt

[54] A. Bigness, S. Vaddypally, M. J. Zdilla, J. L. Mendoza-Cortes, *Coordination Chemistry Reviews* **2022**, *450*, 214168.
[55] G. L. Gutsev, C. A. Weatherford, P. Jena, E. Johnson, B. R. Ramachandran, *J. Phys. Chem. A* **2012**, *116*, 10218–10228.
[56] A. M. Ako, I. J. Hewitt, V. Mereacre, R. Clérac, W. Wernsdorfer, C. E. Anson, A. K. Powell, *Angewandte Chemie International Edition* **2006**, *45*, 4926–4929.
[57] L. Qin, H.-L. Zhang, Y.-Q. Zhai, H. Nojiri, C. Schröder, Y.-Z. Zheng, *iScience* **2021**, *24*, 102350.
[58] M. Manoli, S. Alexandrou, L. Pham, G. Lorusso, W. Wernsdorfer, M. Evangelisti, G. Christou, A. J. Tasiopoulos, *Angewandte Chemie International Edition* **2016**, *55*, 679–684.
[59] S. Kang, H. Zheng, T. Liu, K. Hamachi, S. Kanegawa, K. Sugimoto, Y. Shiota, S. Hayami, M. Mito, T. Nakamura, M. Nakano, M. L. Baker, H. Nojiri, K. Yoshizawa, C. Duan, O. Sato, *Nat Commun* **2015**, *6*, 5955.
[60] S. M. Greer, K. M. Gramigna, C. M. Thomas, S. A. Stoian, S. Hill, *Inorg. Chem.* **2020**, *59*, 18141–18155.
[61] J. A. Chipman, J. F. Berry, *Chem. Rev.* **2020**, *120*, 2409–2447.
[62] D. M. Ermert, J. B. Gordon, K. A. Abboud, L. J. Murray, *Inorg. Chem.* **2015**, *54*, 9282–9289.
[63] E. J. Wucherer, M. Tasi, B. Hansert, A. K. Powell, M. T. Garland, J. F. Halet, J. Y. Saillard, H. Vahrenkamp, *Inorganic Chemistry* **1989**, *28*, 3564–3572.
[64] A. K. Bartholomew, C. E. Juda, J. N. Nessralla, B. Lin, S. G. Wang, Y.-S. Chen, T. A. Betley, *Angewandte Chemie* **2019**, *131*, 5743–5747.
[65] P. L. Dunn, S. Chatterjee, S. N. MacMillan, A. J. Pearce, K. M. Lancaster, I. A. Tonks, *Inorg. Chem.* **2019**, *58*, 11762–11772.
[66] Y. Li, W.-T. Wong, *Coordination Chemistry Reviews* **2003**, *243*, 191–212.
[67] E. Sappa, L. Milone, *Journal of Organometallic Chemistry* **1973**, *61*, 383–388.
[68] J. Fuller, A. Fortunelli, W. A. G. Iii, Q. An, *Phys. Chem. Chem. Phys.* **2019**, *21*, 11444–11454.
[69] J. Qian, Q. An, A. Fortunelli, R. J. Nielsen, W. A. Goddard, *J. Am. Chem. Soc.* **2018**, *140*, 6288–6297.
[70] M. J. Piotrowski, P. Piquini, J. L. F. Da Silva, *Phys. Rev. B* **2010**, *81*, 155446.
[71] J. Wang, Z.-R. Sun, L. Deng, Z.-H. Wei, W.-H. Zhang, Y. Zhang, J.-P. Lang, *Inorg. Chem.* **2007**, *46*, 11381–11389.

Formatted: Font: 8.5 pt

Entry for the Table of Contents

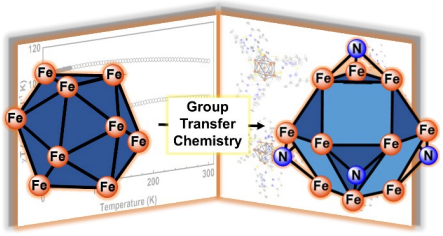

A high nuclearity Fe_{13} cluster with a large room temperature spin value undergoes core structural rearrangement upon group transfer chemistry, as observed by single crystal x-ray diffraction studies.